Int J Clin Exp Pathol 2026;19(5):192-208
www.ijcep.com /ISSN:1936-2625/IJCEP0171860

Original Article

A five-gene mitochondria-associated prognostic signature for bladder cancer

Jing Liu[1], Bo Li[2], Rongrong Hou[3], Jiali Sun[4], Xiaolei Ning[5], Chongni Li[5], Fang Li[5], Lingang Zhang[5]

[1]Pathology Department, Yuncheng Central Hospital, Yuncheng, Shanxi, China; [2]Reproductive Medicine Department, Yuncheng Central Hospital, Yuncheng, Shanxi, China; [3]Maternity Department, Yuncheng Central Hospital, Yuncheng, Shanxi, China; [4]Color Doppler Department, Yuncheng Central Hospital, Yuncheng, Shanxi, China; [5]Emergency Department, Yuncheng Central Hospital, Yuncheng, Shanxi, China

Received February 3, 2026; Accepted April 20, 2026; Epub May 15, 2026; Published May 30, 2026

Abstract: Background: Bladder cancer (BLCA) is a common malignant tumor of the urinary system with a poor prognosis, especially in cases of invasive or advanced patients. Although mitochondrial dysfunction is associated with tumor progression, there are relatively few mitochondrial-related prognostic models for bladder cancer. The intention of study was to construct a five-gene mitochondrial-related prognostic marker for bladder cancer, and perform external validation, and then explore its association with the tumor immune microenvironment and potential immune treatment response. Methods: Transcriptome and clinical data were obtained from TCGA and GEO databases - intersecting bladder cancer-related differentially expressed genes (BLCA-related DEGs) with the mitochondrial-related gene database (MitoCarta 3.0 genes) to find the mitochondria-related differentially expressed genes (Mitochondria-related DEGs). Construction of a prognosis model using univariate (uni), lasso, and multivariate Cox regression analyses, was used for verificaiotn in 2 gene expression profile public databases (GEO cohorts). Functional enrichment (func enrich), tumor microenvironment (tumor microenv), immune infiltration (immune infil), mutation (mut), and single-cell transcriptomic analyses were carried out. Results: A prognosis model was created containing five genes: COX7A1, MTHFD1L, MTG1, SCO2, and ACP6. The survival rate of high-risk patients was found to be poorer compared with that of low-risk patients. The high-risk tumor stromal score was higher, the fibroblast-related characteristics were enriched, with differences in the immune pattern. Single-cell analysis found COX7A1 in endothelial cells and mast cells, MTHFD1L in T cells, and SCO2 in endothelial cells. Functional analysis associated the high-risk group with extracellular matrix remodeling, stromal activation, and changes in immune pathways. This model also has potential value in estimating the response to immunotherapy. Conclusions: A five-gene prognosis marker related to mitochondria for bladder cancer was developed and verified. This model may become a useful tool for survival stratification of bladder cancer patients and characterization of tumor microenvironment heterogeneity.

Keywords: Poor mitochondrial function in bladder cancer, prognosis marker, tumor microenvironment, immunotherapy, single-cell analysis

Introduction

Bladder cancer is a common urological malignancy and an important cause of cancer-related morbidity and mortality worldwide. The prognosis is relatively poor for patients with muscle-invasive bladder cancer and advanced diseases. Recurrence, progression and other situations, as well as local invasion, distant metastasis and drug resistance, affect the clinical course of the disease. Serious complications such as urinary tract obstruction, hydronephrosis, renal dysfunction and organ dysfunction related to metastasis make the prognosis worse. These challenges mean that reliable biomarkers are needed to improve the prognosis and assist in treatment [1]. Recent studies have found that bladder cancer (BLCA) is heterogeneous, and changes occur in cell cycle, metabolism, redox, apoptosis and tumor microenvironment. Mitochondrial dysfunction has received significant attention. The function of mitochondria lies in tube ATP generation, oxidative stress and programmed cell death. Functional problems may cause tumor cell survival, because their metabolism can adapt and resist treat-

https://doi.org/10.62347/RKHD2558

ment. Previous studies have mentioned that mitochondrial-related genes may relate information on the prognosis of bladder cancer, but the evidence is not sufficient and needs to be further verified [2, 3]. The tumor microenvironment (TME) is also crucial for the progression and treatment response of bladder cancer. Stromal cells, immune cells, extracellular matrix components and soluble mediators jointly affect tumor behavior. Immune checkpoint blockade has improved the prognosis of some bladder cancer patients, but the persistent benefits vary. Observations show that Conv markers are not sufficient to capture tumor-immune interactions [4-7]. Therefore, in the present study, we developed and externally validated a five-gene mitochondria-associated prognostic signature for bladder cancer. We further investigated its associations with overall survival, stromal and immune characteristics of the TME, mutation patterns, and potential responsiveness to immunotherapy.

Methods

Data collection

Transcriptomic and clinical data for bladder cancer were obtained from publicly available databases. The TCGA-BLCA cohort was used as the training set, and two GEO cohorts, GSE31684 and GSE32894, were used for external validation. These datasets were selected because they contained gene expression profiles and survival information suitable for prognostic modeling. The TCGA database (https://www.cancer.gov/tcga) included RNA-seq data from 431 BLCA samples. The validation datasets were downloaded from GEO (https://www.ncbi.nlm.nih.gov/geo/), including 93 samples from GSE31684 and 308 samples from GSE32894. A list of mitochondria-related genes was retrieved from the MitoCarta 3.0 database (https://www.broadinstitute.org/) [8].

The inclusion criteria were as follows: (1) bladder cancer samples with available gene expression data; and (2) samples with complete survival information for prognostic analysis. Experiments with duplicate samples, missing survival time/status samples, and incomplete risk score calculation information are excluded. Normal tissue samples were only used for differential expression analysis and not for constructing survival models.

Detection of differentially expressed genes (DEGs)

In R (version 1.38.3), "DESeq2" was used to identify differentially expressed genes (DEGs) between normal/tumor samples and high/low-risk groups in the training cohort. The screening criteria were: |log2 fold change| > 1 and adjusted *P*-value < 0.05. The "ggplot2" package was used to draw a volcano plot; the overlap of differentially expressed genes (DEGs) and mitochondrial-related genes was visualized using a Venn diagram. Heatmaps were used to show the expression status of differentially expressed genes between normal tissues and tumor tissues.

Construction and verification of a mitochondrial-related prognostic model

First, univariate Cox regression was used to screen out mitochondrial-related genes related to overall survival. LASSO regression was used to reduce the number of candidate genes. A prognostic model was used with multivariate Cox regression analysis. The risk score of each patient was calculated according to the sum of gene expression multiplied by the relevant regression coefficient. 'Exp value' refers to the gene expression in the feature, and 'coef' refers to the relevant regression coefficient. The training cohort was divided into a high-risk group and low-risk group according to the median risk score, and the verification cohort was processed by the same formula. The prognostic performance of the model was evaluated using Kaplan-Meier survival analysis, time-dependent receiver operating characteristic (ROC) analysis, risk distribution plots, survival status plots, and the concordance index (C-index).

Construction and evaluation of the nomogram

To determine whether the risk score was an independent predictor of survival, univariate Cox regression analysis was first performed for the risk score and available clinical variables, including age, sex, T stage, N stage, M stage, tumor stage, race, and vital status. Variables with prognostic significance were then included in multivariate Cox regression

analysis. Independent predictors were incorporated into a nomogram to estimate the probabilities of 1-, 3-, and 5-year overall survival. The predictive performance of the nomogram was assessed using ROC curves, calibration plots, and decision curve analysis (DCA).

Gene ontology (GO) and Kyoto Encyclopedia of Genes and Genomes (KEGG) analyses

Functional enrichment analysis of mitochondria-related DEGs and DEGs between the high-risk and low-risk groups was performed using the R packages "clusterProfiler", "org.Hs.eg.db", "enrichplot", and "ggplot2" (version 3.5.1). Pathways with adjusted $P < 0.05$ were considered significantly enriched [9, 10].

Gene set enrichment analysis (GSEA)

Gene set enrichment analysis was performed using gene sets downloaded from the GSEA website (https://www.gsea-msigdb.org/gsea/index.jsp). This analysis was used to identify pathways preferentially enriched in the high-risk and low-risk groups.

Tumor microenvironment analysis

The ESTIMATE algorithm was implemented using the "estimate" R package (version 3.5.1) to calculate stromal scores. Gene set enrichment analysis was then used to generate a panel of biomarkers associated with the tumor microenvironment [11, 12].

Quantification of immune cell infiltration and evaluation of immunotherapy-related indicators

The relative abundance of 22 tumor-infiltrating immune cell subtypes in BLCA samples was estimated using the CIBERSORT algorithm. Differences in immune cell infiltration between the high-risk and low-risk groups were compared using the Wilcoxon rank-sum test [13]. Immune scores and tumor purity were further assessed using the ESTIMATE algorithm. Immunophenotype score (IPS) data were obtained from The Cancer Immunome Atlas (https://tcia.at/home). Tumor immune dysfunction and exclusion (TIDE) scores and tumor mutational burden (TMB) scores were also calculated to estimate potential responsiveness to immunotherapy [14, 15].

Mutation analysis

Somatic mutation data were obtained from the cBioPortal database (https://www.cbioportal.org/) [16, 17]. The "maftools" R package (version 3.5.1) was used to calculate the TMB score for each sample and to generate waterfall plots showing the mutation landscape of BLCA patients in the high-risk and low-risk groups.

Processing of scRNA-seq data

Single-cell RNA sequencing data were analyzed using Seurat (version 4.3.0) according to standard procedures for quality control, normalization, dimensionality reduction, clustering, and annotation [18]. Quality control was performed as described in previous studies [19]. After initial filtering, the analysis pipeline included regression of cell-cycle effects, normalization, dimensionality reduction, cell clustering at a resolution of 1.0, and systematic cell type annotation.

Statistical analysis

All statistical analyses were performed using R software (version 4.2.3). Continuous variables are expressed as mean ± standard deviation (SD) for normally distributed data or as median (interquartile range, IQR) for non-normally distributed data, as appropriate. Categorical variables are expressed as number (percentage). Comparisons between two groups were performed using Student's t test or the Wilcoxon rank-sum test, as appropriate. The chi-square test was used to compare categorical variables. Correlations between variables were assessed using Spearman's correlation analysis. The concordance index (C-index) was calculated to evaluate predictive performance for overall survival. A two-sided P value < 0.05 was considered statistically significant.

Results

Identification of mitochondria-associated DEGs and functional enrichment in BLCA

The overall workflow of the present study is shown in **Figure 1**. A total of 4,722 DEGs, including 4,597 protein-coding genes, were identified between tumor and normal tissues and visualized by a volcano plot (**Figure 2A**). After inter-

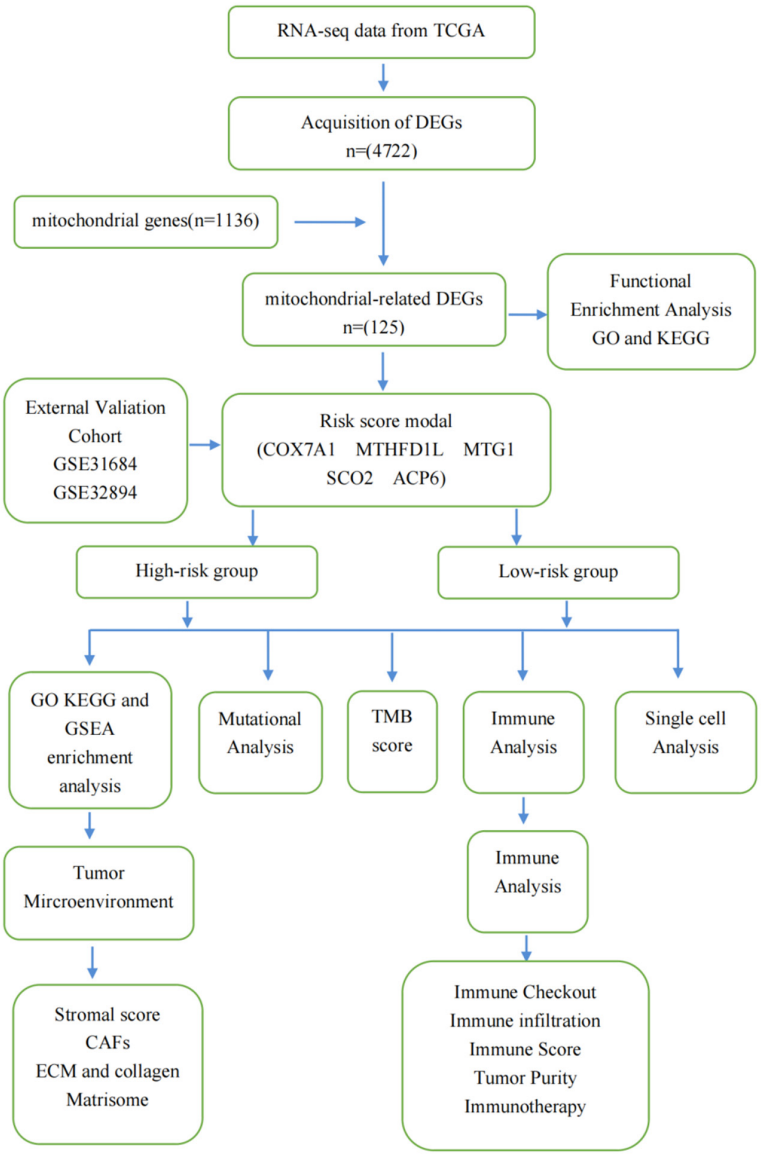

Figure 1. Flowchart diagram of this study.

secting these genes with mitochondria-related genes, 125 candidate mitochondria-associated DEGs were obtained (**Figure 2B**). A heatmap further illustrated the differences in gene expression between tumor and normal tissues (**Figure 2G**).

To explore the biological roles of these mitochondria-associated DEGs, GO enrichment analysis was performed. The enriched terms suggested involvement in mitochondrial organization and small-molecule catabolic processes. In the cellular component category, these genes were mainly associated with the mitochondrial outer membrane and mitochondrial matrix.

Development and validation of a mitochondria-associated risk signature

Among the 125 mitochondria-associated DEGs, 27 genes were identified as potential prognostic factors by univariate Cox regression analysis ($P < 0.05$, **Figure 2C**). LASSO regression reduced the number of candidate genes to 18, and multivariate Cox regression further narrowed them to five genes (**Figure 2D**, **2E**). The final prognostic model consisted of COX7A1, MTHFD1L, MTG1, SCO2, and ACP6. Compared with normal tissues, tumor tissues showed lower expression of COX7A1 and higher expression of MTHFD1L, MTG1, SCO2, and ACP6 (**Figure 2F**).

Based on the median risk score, patients in the TCGA-BLCA cohort were divided into high-risk and low-risk groups. Kaplan-Meier analysis showed that patients in the high-risk group had significantly worse overall survival than those in the low-risk group ($P = 8.1702e-05$, **Figure 3A**). Time-dependent ROC analysis yielded AUC values of 0.640, 0.657, and 0.664 for predicting 1-, 3-, and 5-year overall survival, respectively (**Figure 3B**). **Figure 3C** presents the risk score distribution, survival status, and expression patterns of the five genes in the training cohort. Together, these results indicate that the model had acceptable prognostic performance in the TCGA cohort.

The robustness of the model was then tested in the external validation cohorts. In GSE31684, patients in the high-risk group again showed significantly worse survival ($P < 0.0001$, **Figure 3D**, **3E**), and the AUC values for predicting 1-,

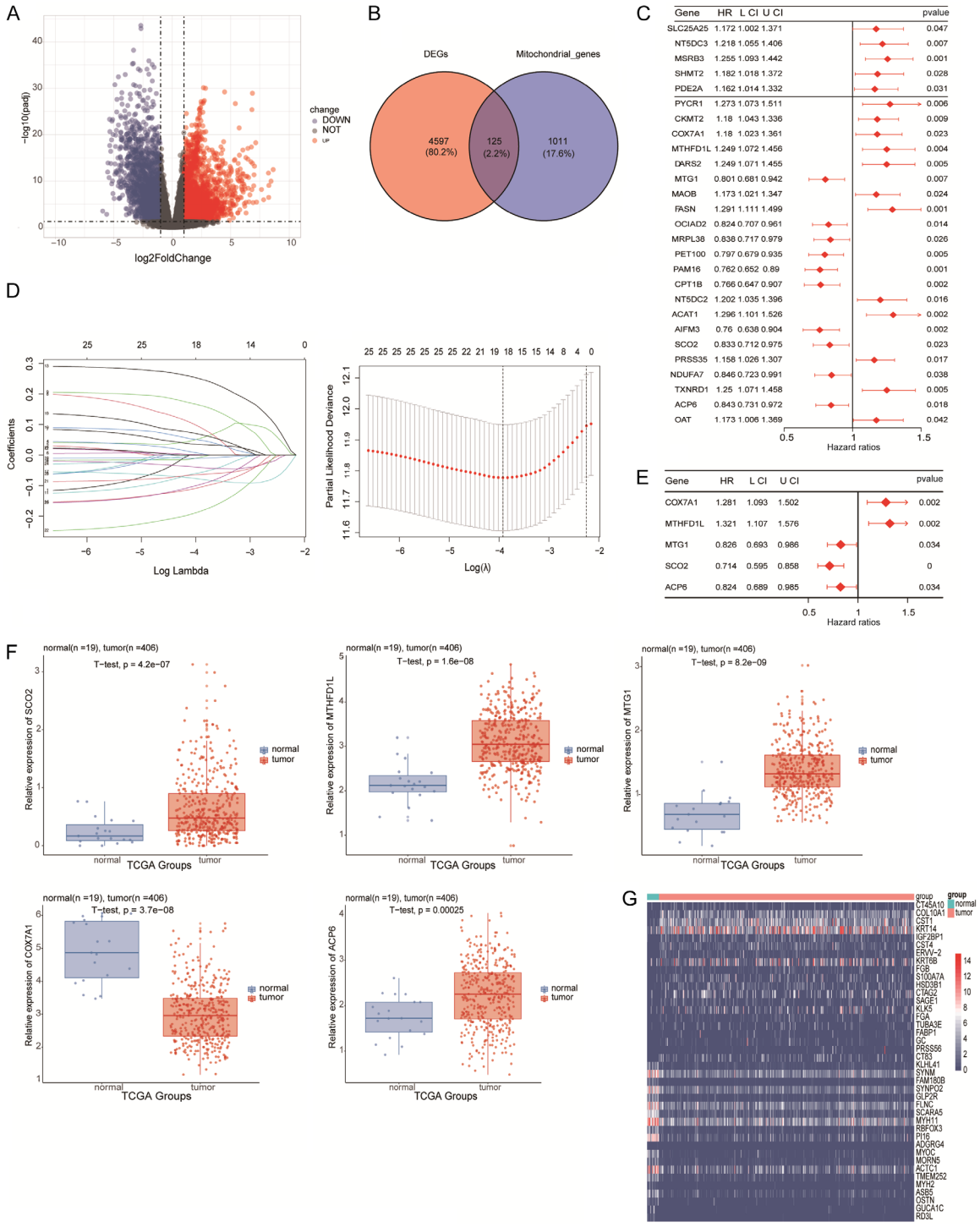

Figure 2. Identifying mitochondrion-related DEGs and building a prognostic risk model using the TCGA-BLCA cohort. A. Volcano plot of 4,722 DEGs in the BLCA tumor and normal groups. B. The overlap of 4,722 DEGs and 1136 mitochondrial genes led to the identification of 125 hub genes, as shown in the Venn diagram. C. Twenty-seven genes were associated with prognosis in patients with BLCA according to univariate Cox regression analysis. D. LASSO regression was performed on the 27 OS-related genes, with cross-validation used to select the optimal tuning parameter. The x-axis represents the log(λ) values, whereas the y-axis represents the partial likelihood deviance. The red dots in the figure indicate the partial likelihood deviance ± standard error for various tuning parameters. E. Multivariable Cox regression analysis identified 5 genes that are associated with the prognosis of patients with BLCA. F. Gene expression levels of the 5 prognosis-related genes identified in the TCGA-BLCA study. G. Hotspot map of the top 20 upregulated and downregulated DEGs between the BLCA tumor and normal groups.

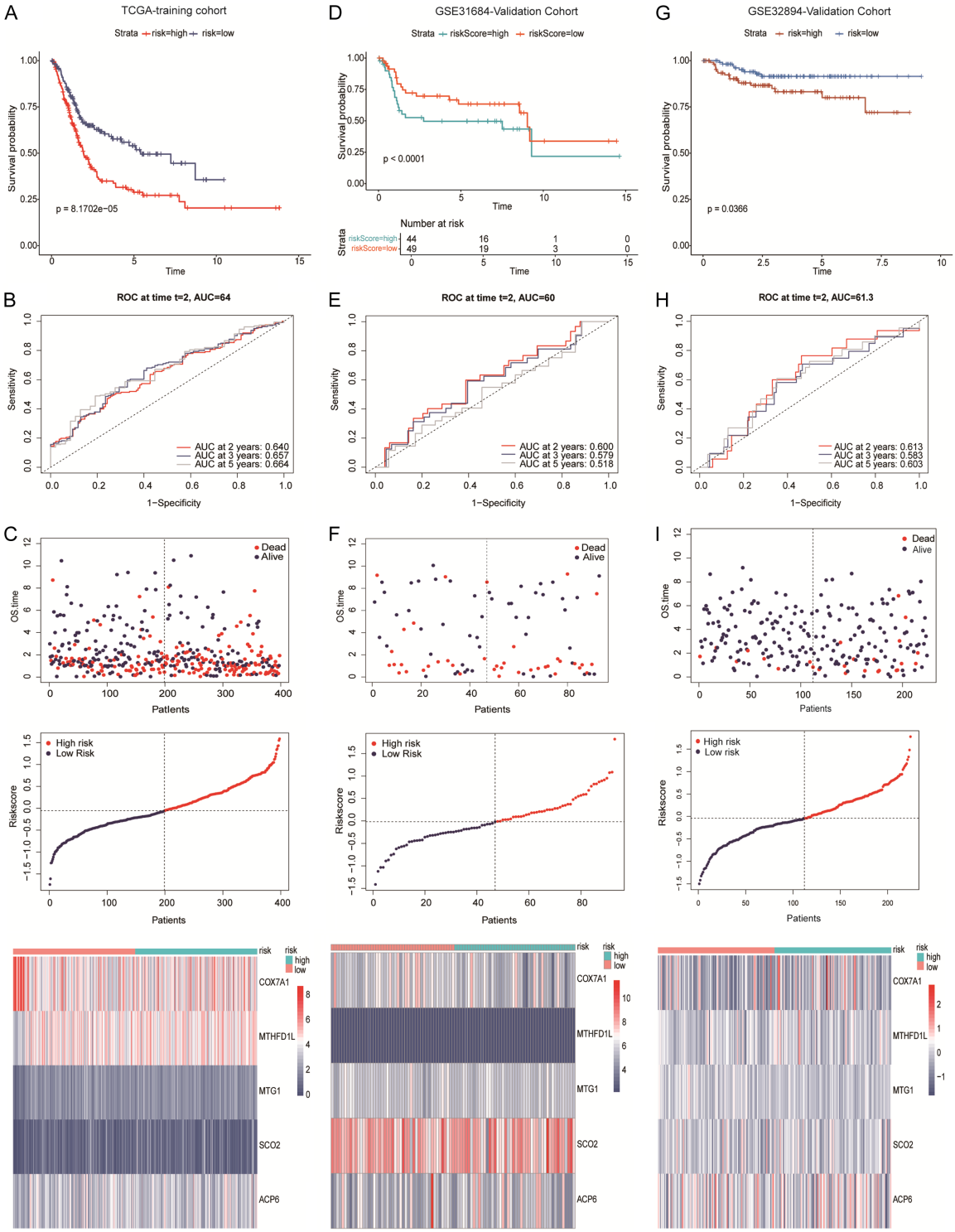

Figure 3. Performance of the prognostic risk model in the training and validation cohorts. (A, D, G) Kaplan-Meier survival curves depicting OS in the high- and low-risk groups for the TCGA-BLCA training cohort (A), the GSE31684 validation cohort (D) and the GSE32894 validation cohort (G). (B, E, H) ROC analysis for estimating 1-, 3-, and 5-year OS in the TCGA-BLCA training set (B), the GSE31684 validation set (E) and the GSE32894 validation set (H). (C, F, I) Visualization of the risk score distribution, survival status (red dots represent deceased genes, blue dots represent surviving genes), and expression patterns of the five model genes in the TCGA-BLCA training cohort (C), the GSE31684 validation set (F), and the GSE32894 validation set (I).

Table 1. Clinical characteristics between the low-risk and high-risk groups

Variables	High risk 192	Low risk 171	p
Age mean (SD)	69.47 (9.91)	66.62 (11.21)	**0.011**
Gender (%)			0.201
Female	55 (28.6)	38 (22.2)	
Male	137 (71.4)	133 (77.8)	
M_stage (%)			**< 0.001**
M0	72 (37.5)	105 (61.4)	
M1	7 (3.6)	1 (0.6)	
MX	113 (58.9)	65 (38.0)	
N_stage (%)			0.09
N0	106 (55.2)	111 (64.9)	
N1	25 (13.0)	18 (10.5)	
N2	46 (24.0)	26 (15.2)	
N3	4 (2.1)	1 (0.6)	
NX	11 (5.7)	15 (8.8)	
T_stage (%)			**0.001**
T0	0 (0.0)	1 (0.6)	
T1	1 (0.5)	2 (1.2)	
T2	11 (5.7)	26 (15.2)	
T2a	5 (2.6)	18 (10.5)	
T2b	25 (13.0)	29 (17.0)	
T3	21 (10.9)	22 (12.9)	
T3a	44 (22.9)	24 (14.0)	
T3b	51 (26.6)	30 (17.5)	
T4	6 (3.1)	3 (1.8)	
T4a	25 (13.0)	14 (8.2)	
T4b	3 (1.6)	2 (1.2)	
Stage (%)			**< 0.001**
Stage I	1 (0.5)	1 (0.6)	
Stage II	34 (17.7)	67 (39.2)	
Stage III	80 (41.7)	57 (33.3)	
Stage IV	77 (40.1)	46 (26.9)	
Race (%)			**0.002**
Asian	11 (5.7)	31 (18.1)	
Black or African American	9 (4.7)	10 (5.8)	
Not reported	10 (5.2)	6 (3.5)	
White	162 (84.4)	124 (72.5)	
vital_status (%)			**< 0.001**
Alive	89 (46.4)	112 (65.5)	
Dead	103 (53.6)	59 (34.5)	

Note: Bold indicates P ≤ 0.05.

3-, and 5-year overall survival were 0.600, 0.579, and 0.518, respectively. Risk score distribution, survival status, and gene expression patterns are shown in **Figure 3F**. In GSE32894, the high-risk group also had significantly poorer survival than the low-risk group (P = 0.0366, **Figure 3G**), with AUC values of 0.613, 0.583, and 0.603 for 1-, 3-, and 5-year survival, respectively (**Figure 3H**). The corresponding risk distribution, survival status, and gene expression patterns are shown in **Figure 3I**. These findings support the generalizability of the five-gene signature across independent BLCA cohorts.

Comparison of clinical characteristics between the two risk groups showed no significant differences in sex, N stage, or tumor stage. Significant differences were observed in age (P = 0.011), M stage (P < 0.001), T stage (P = 0.001), overall stage (P < 0.001), vital status (P < 0.001), and race (P = 0.002) (**Table 1**).

Functional enrichment analysis of DEGs between the high-risk and low-risk groups

GO enrichment analysis of DEGs between the high-risk and low-risk groups indicated significant enrichment in biological processes related to leukocyte migration, cell chemotaxis, and muscle tissue development. In the composition categories of cells, sarcomeres, myofibrils and contractile fibers are gathered in large numbers. Molecular function analysis finds that there are aggregations in terms of growth factor, cytokine activity and integrin binding (**Figure 4A**). The gene ontology (GO) chord diagram also shows obvious aggregations in extracellular matrix organization, cell-matrix adhesion, wound healing, collagen fiber organization and basement membrane organization. The key genes in these pathways include COL3A1, ADAMTS12, TGFB3, PDGFRB and THBS1, which indicates that they play important roles in matrix remodeling, cell adhesion and tissue repair (**Figure 4**). KEGG enrichment analysis found obvious pathways, such as "ECM-

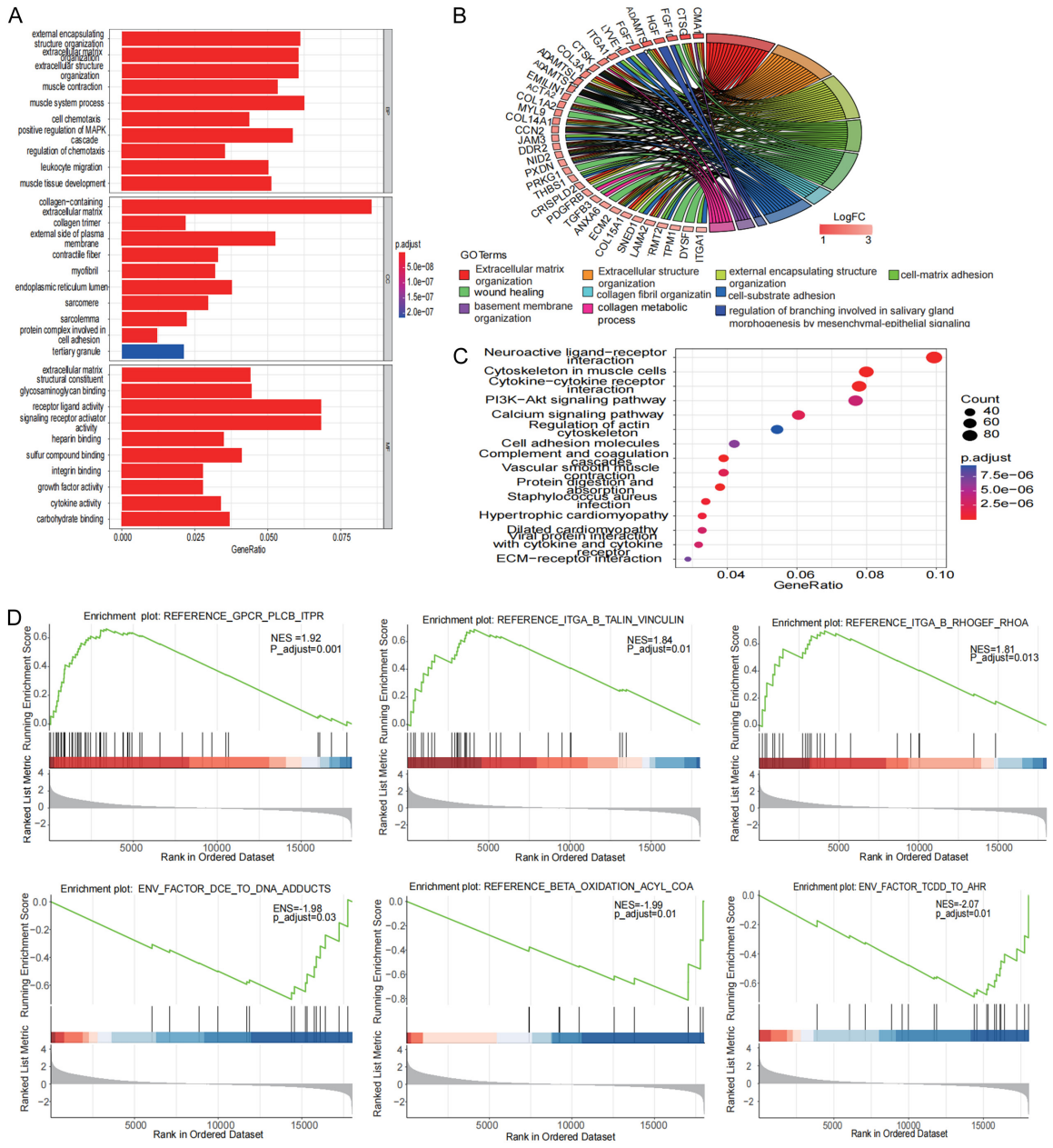

Figure 4. Enrichment analysis of the high-risk and low-risk groups. A. Bar plot. Diagram showing important GO pathways, including biological processes (BP), cellular components (CC) and molecular functions (MF). B. Circle map. Bands with different colors in the right half of the circle represent the top 10 significantly enriched GO pathways, while the left half displays the genes associated with these pathways, illustrating their functional involvement. C. Bubble chart. Bubble plots displaying the results of the KEGG-enriched pathways. D. GSEA indicates the expression of different sets of genes in the high- and low-risk groups.

receptor interaction". There were also additional enriched pathways, such as "dilated cardiomyopathy", indicating that extracellular matrix remodeling may be related.

GSEA showed suppression of the DCE-induced DNA adduct pathway and activation of the GPCR-PLCB-ITPR signaling pathway, suggesting altered DNA damage responses and enhanced calcium-related signaling in the high-risk group (**Figure 4D**).

Association between the mitochondria-associated risk score and TME signatures in BLCA

Given that functional analysis highlighted pathways related to the tumor microenvironment, we next examined the association between the

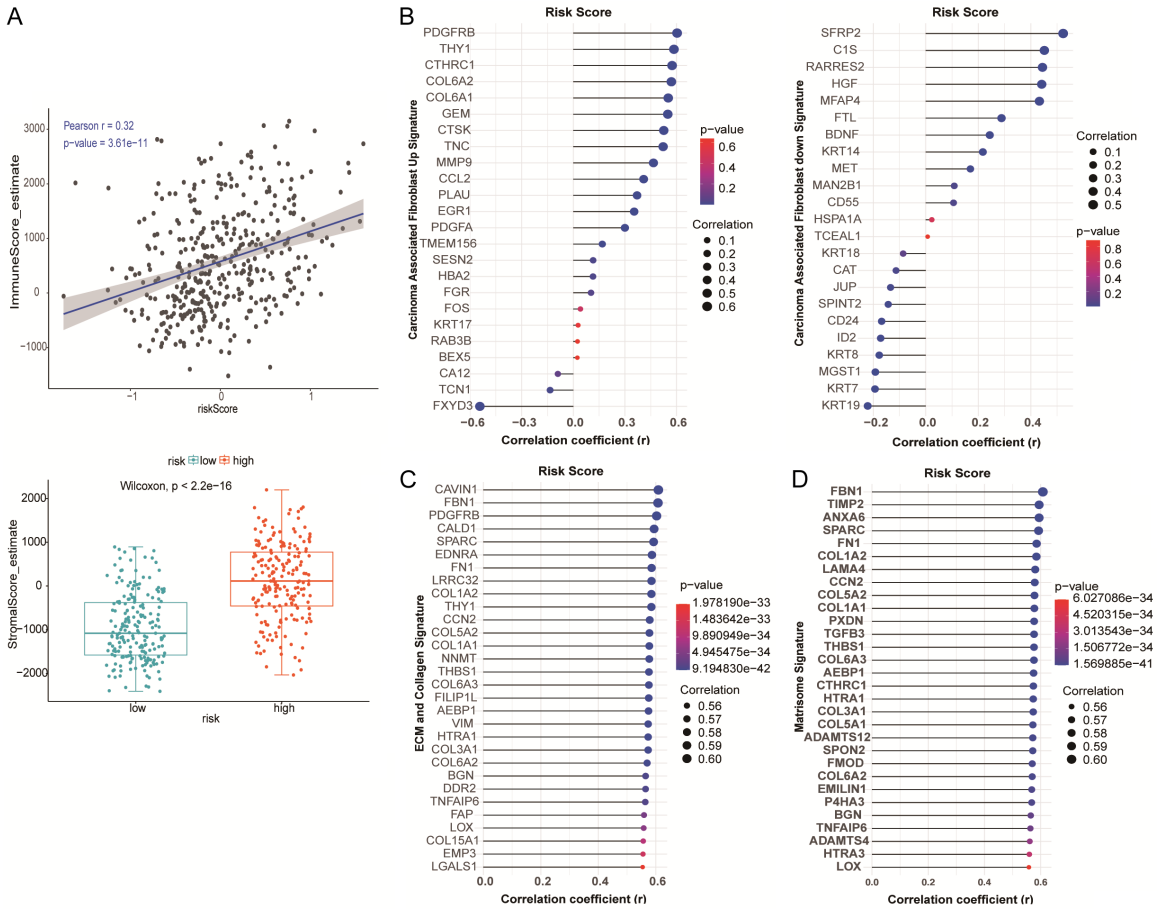

Figure 5. The risk score was significantly associated with the TME signatures in BLCA. A. Correlation between the stromal score and risk score and distribution between the low- and high-risk groups. B. Correlation analysis of the risk score and carcinoma-associated fibroblast (CAF) up- and downregulated signature expression. C. Analysis of the correlation between the risk score and the expression of the ECM and collagen signatures. D. Analysis of the correlation between the risk score and the expression of the matrisome signatures.

risk score and TME-related signatures. A strong positive association was observed between the risk score and stromal score, and the high-risk group had significantly higher stromal scores than the low-risk group (**Figure 5A**).

Further analysis showed that the risk score was positively correlated with most fibroblast-related signatures, including both upregulated and downregulated carcinoma-associated fibroblast gene sets (**Figure 5B**). Positive correlations were also observed between the risk score and matrisome-related as well as ECM/collagen-related signatures (**Figure 5C**, **5D**). These findings indicate that the mitochondria-associated risk score is closely linked to stromal activation and extracellular matrix remodeling in BLCA.

The mitochondrial risk score is associated with immunity and therapy response in BLCA

Because tumor immune microenvironment features are closely related to prognosis and treatment response, we further investigated the association between the risk score and immune cell infiltration. CIBERSORT analysis showed that the high-risk group had significantly higher levels of activated CD4 memory T cells, M0 macrophages, M1 macrophages, and M2 macrophages. In contrast, the low-risk group showed higher levels of monocytes, activated dendritic cells, CD8 T cells, follicular helper T cells, and regulatory T cells (Tregs) (**Figure 6A**).

Correlation analysis showed that there was a moderate positive correlation between the risk

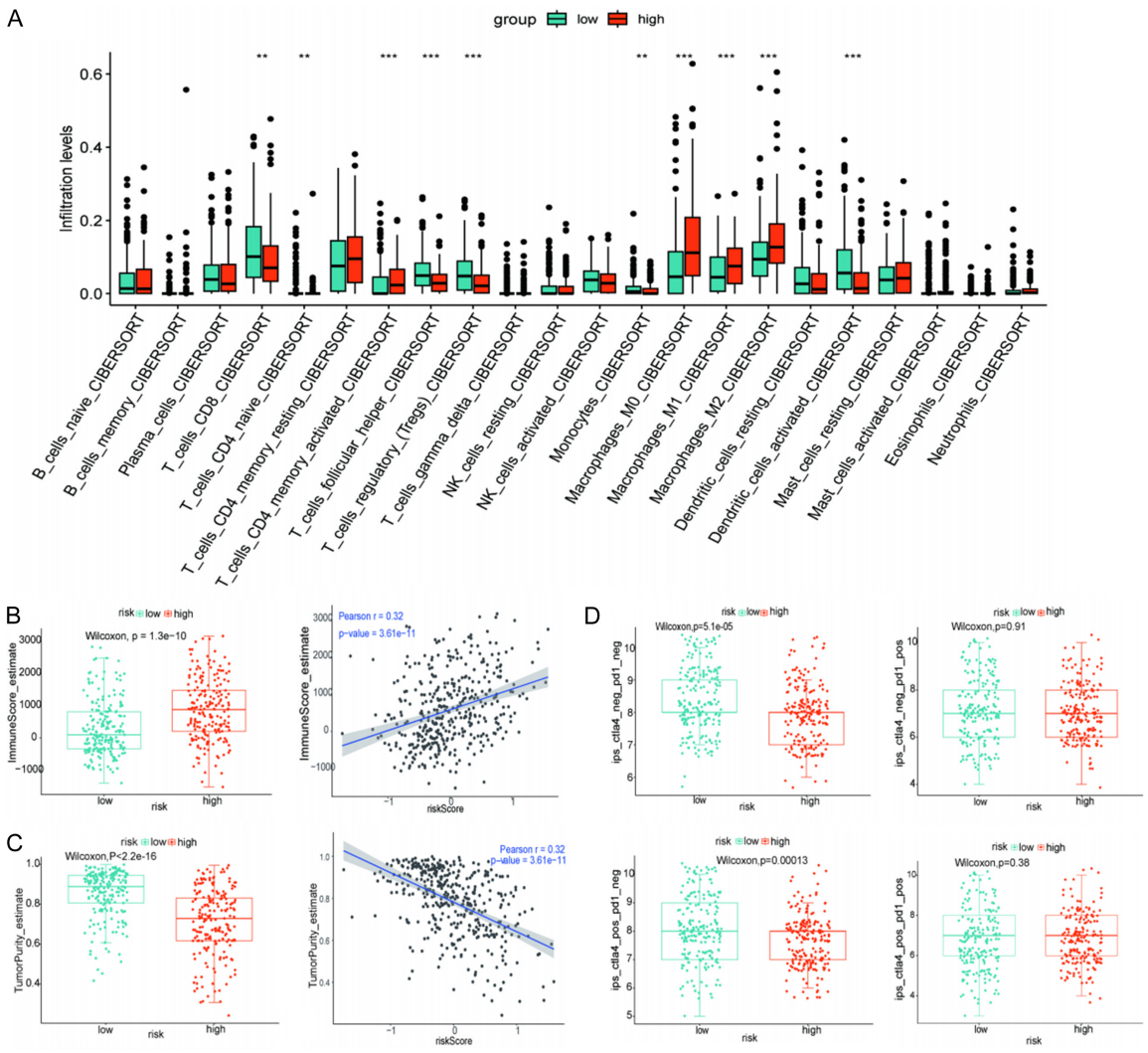

Figure 6. Comparative analysis revealed distinct immune profiles between the low- and high-risk subgroups within the TCGA-BLCA cohort. A. CIBERSORT analysis. B, C. Correlations of risk scores with immune scores and tumor purity. D. The immunophenotype score (IPS) was analyzed for different risk groups.

score and the immune score (Pearson correlation coefficient r = 0.32, P = 3.61e-11). There was a significant difference in the immune score between the two groups of risks (Wilcoxon test, P = 1.3e-10), indicating the presence of different immune microenvironments. The correlation between the risk score and tumor purity was weak and not statistically significant (Pearson correlation coefficient r = 0.32, P = 0.26), and the tumor purity of the high-risk group was lower than that of the low-risk group (Wilcoxon test, P < 2.2e-16) (**Figure 6B**, **6C**). IPS analysis found differences in the risk groups. The low-risk group has a higher IPS in the CTLA4 negative/PD1 negative (P = 5.1e-05) and CTLA4 positive/PD1 negative (P = 0.00013) subgroups; CTLA4 positive/PD1 positive (P = 0.38) or CTLA4 negative/PD1 positive (P = 0). These findings in **Figure 6D** suggest that the association between risk stratification and immune activation may differ depending on the checkpoint expression status. We then applied the TIDE algorithm to estimate the predictive value of the risk score for immunotherapy response. The low-risk group had a significantly higher response rate than the high-risk group (P < 0.001), and the proportion of responders differed markedly between the two groups (**Figure 7A**). Patients with lower immune scores showed higher response rates than those with higher immune scores (P < 0.01) (**Figure 7B**). Within the low-immune-score subgroup, the

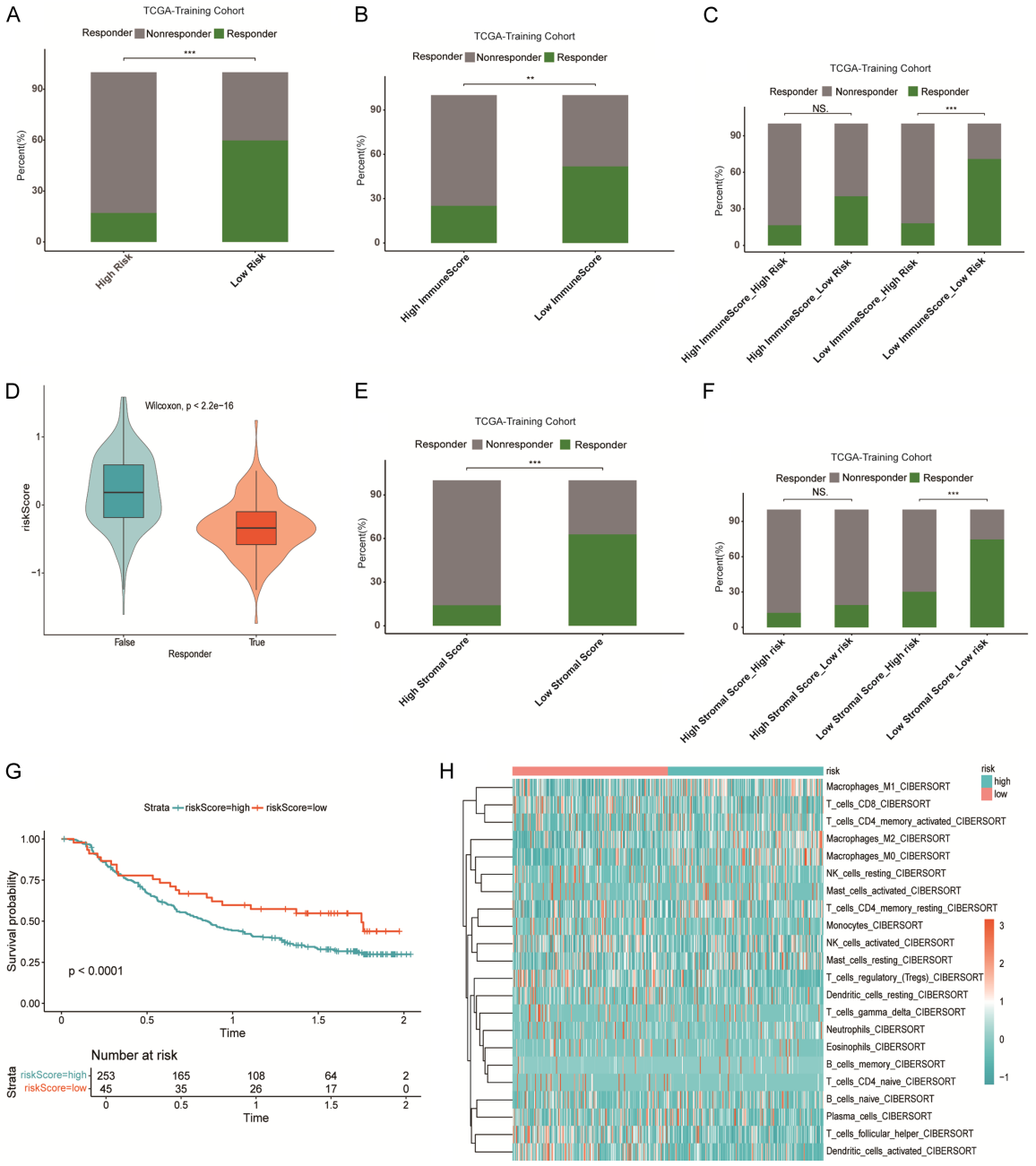

Figure 7. The risk score serves as a potential biomarker for predicting the therapeutic benefits of immune treatments in BLCA. A. Comparison of immune treatment response rates between the high-risk and low-risk groups. B. Association between immune score and immune treatment response rate. C. Proportion of patients in the four groups according to the risk score and immune score who responded to immunotherapy. D. Distribution of risk scores between responders and nonresponders. E. Association between the stromal score and immune treatment response rate. F. Proportion of patients in the four groups according to the risk score and stromal score who responded to immunotherapy. G. Kaplan-Meier survival analysis of the high-risk and low-risk groups in the IMVigor210 cohort. H. Heatmap of gene expression profiles across different risk and stromal score groups.

response rate was significantly higher in the low-risk group than in the high-risk group (P < 0.001) (**Figure 7C**). Responders had significantly lower risk scores than nonresponders (Wilcoxon test, P < 2.2e-16) (**Figure 7D**). Similarly, patients with lower stromal scores had higher response rates than those with higher stromal scores (P < 0.001) (**Figure 7E**), and among patients with low stromal scores, the low-risk group showed a significantly higher

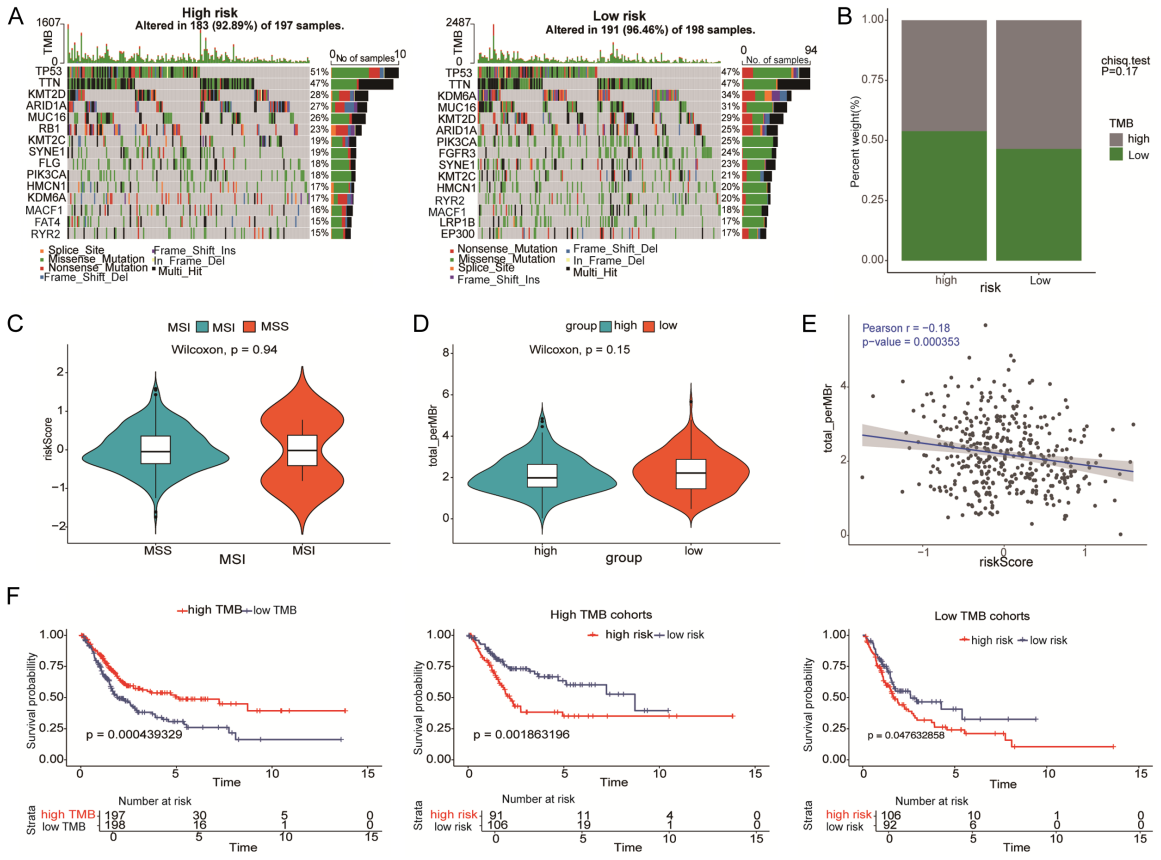

Figure 8. Genomic and prognostic analysis of mutations in the high- and low-risk groups. A. Mutational landscape of BLCA in the high-risk and low-risk groups, highlighting frequently mutated genes. B. Comparison of TMB between the high- and low-risk groups. C. Distribution of risk scores between the microsatellite stable (MSS) and microsatellite instability (MSI) subgroups. D. Relationships between the risk score and the total number of mutations. E. Correlation analysis between the risk score and TMB, which revealed a significant negative correlation. F. Kaplan-Meier survival analysis comparing overall survival (OS) in the high- and low-TMB groups (left), as well as survival differences stratified by risk score within the high-TMB (middle) and low-TMB (right) subgroups.

response rate than the high-risk group ($P < 0.001$) (**Figure 7F**).

Validation in the IMVigor210 cohort further showed that high-risk patients had significantly poorer survival than low-risk patients ($P < 0.0001$, **Figure 7G**). Gene expression patterns across stromal score and risk score groups are shown in **Figure 7H**. Taken together, these results indicate that the risk score is associated with immune context and may be useful for estimating immunotherapy responsiveness.

Mutation landscape of BLCA patients in the high-risk and low-risk groups

To examine the relationship between genetic alterations and risk stratification, we analyzed somatic mutation patterns in the two risk groups. Different mutation spectra could be seen through comparative genomic analysis; the high-risk group had a significantly higher frequency of alterations in tumor suppressor genes, especially TP53 ($P < 0.001$). The low-risk group has an advantage mutation in mucin-encoding genes such as MUC16 ($P = 0.003$) (**Figure 8A**). There is no significant difference in the distribution of TMB categories between the two groups, although there is a difference in mutation patterns (tested by chi-square, $P = 0.17$) (**Figure 8B**). Similarly, there was no obvious association between MSI status and risk stratification (t-test, $P = 0.94$) (**Figure 8C**). There was also no difference in the quantitative analysis of the total number of mutations between the two groups (Mann-Whitney U test, $P = 0.15$) (**Figure 8D**). Correlation analysis showed a weak but significant negative correlation between the risk score and tumor mutation burden (TMB), with a Pearson correlation coefficient r of 0.18 and a *P* value of 0.00035 (**Figure**

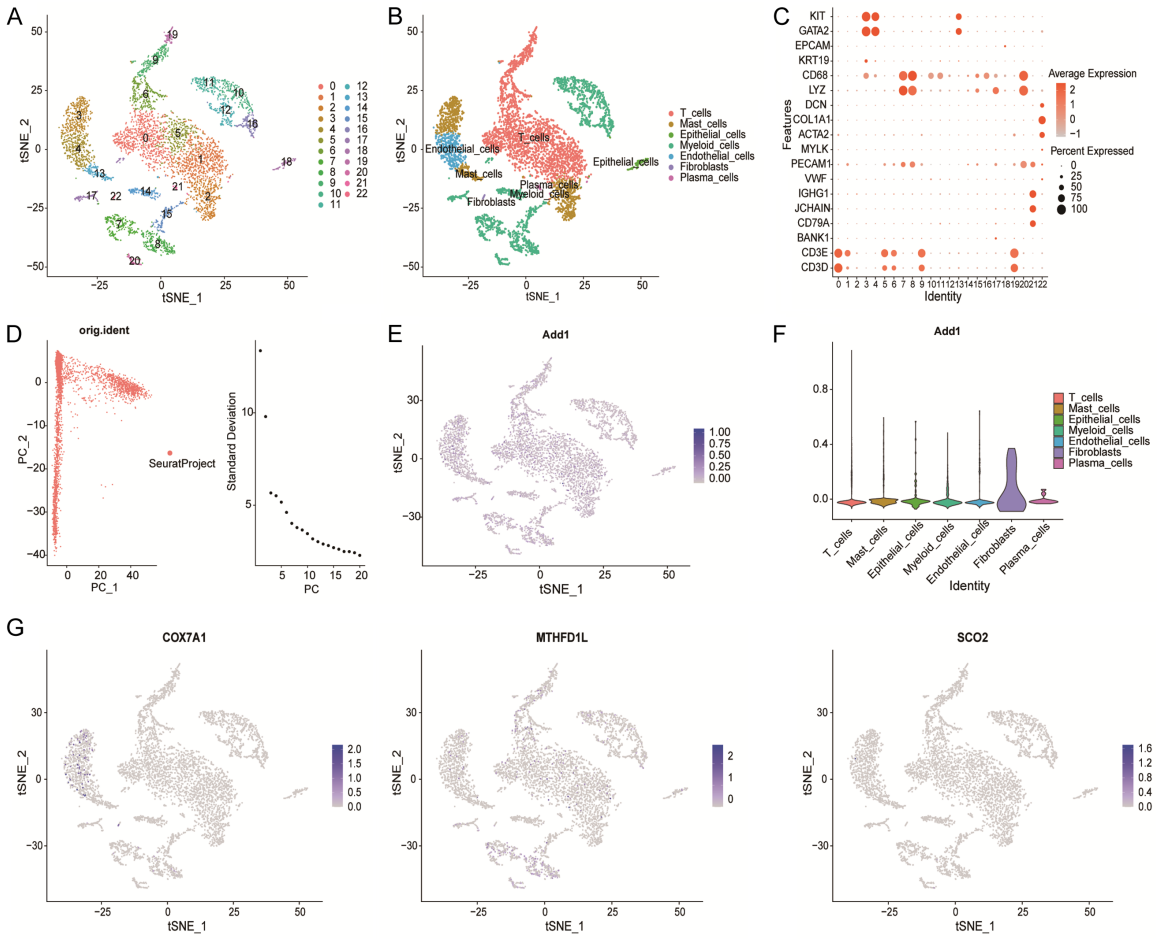

Figure 9. Single-cell transcriptomic analysis reveals distinct cell populations and gene expression patterns. A. t-SNE plot showing the clustering of single cells into distinct populations. B. Annotation of cell types on the basis of known marker genes, identifying T cells, mast cells, epithelial cells, myeloid cells, endothelial cells, fibroblasts, and plasma cells. C. Dot plot displaying the expression levels and proportions of representative marker genes across different cell types. D. Principal component analysis (PCA) showing the variance distribution and major contributors to cellular heterogeneity. E. In the Et-SNE plot, the Add1 gene set score is mainly enriched in fibroblasts. F. The violin plot confirms that the Add1 gene set score in fibroblasts is higher than in other cells. G. In the Gt-SNE plot, the cell type-specific expression patterns of COX7A1, MTHFD1L, and SCO2 are presented: COX7A1 is enriched in endothelial and mast cells, MTHFD1L is in T cells, and SCO2 is in endothelial cells.

8E). In survival analysis, the overall survival (OS) of patients with high tumor mutation burden (TMB) is better than that of patients with low TMB (log-rank test, P = 0.00044). In the high-TMB and low-TMB subgroups, the survival status of high-risk patients is worse than that of low-risk patients (P = 0.0019 and P = 0.048) (see **Figure 8F**). The prognostic value of the risk model still exists in the TMB stratification [20-22].

Single-cell RNA sequencing found that cell types have specific gene expression patterns

The cellular environment of the sig gene was explored and analyzed for the data of single-cell RNA sequencing (scRNA-seq). t-SNE clustering was used to find different cell populations (T cells, mast cells, epithelial cells, myeloid cells, endothelial cells, fibroblasts, plasma cells) and annotate them according to known marker genes (**Figure 9A**, **9B**). The dot plot of representative marker genes further illustrates the specific expression patterns of cell types: COL1A1, ACTA2 in fibroblasts; EPCAM, KRT19 in epithelial cells; IGHG1, JCHAIN in plasma cells (**Figure 9C**). Principal component analysis (PCA) identified the main contributing factors to cellular heterogeneity (**Figure 9D**). Gene set scoring analysis reveals that Add1 is preferentially enriched in fibroblasts, which is confirmed by violin plot analysis

(**Figure 9F**). The genes visualized by t-SNE have cell-type-specific expression (**Figure 9E**). COX7A1 is enriched in endothelial cells and mast cells, MTHFD1L is in T cells, and SCO2 is in endothelial cells (**Figure 9G**). These findings suggest that the model genes may play different biological roles in different cellular components of the tumor microenvironment.

Discussion

In this study, a mitochondrial-related five-gene prognostic signature (sig) for bladder cancer was constructed, and the performance of this signature was verified in two independent GEO cohorts. The risk score of this model is significantly associated with overall survival, stromal activation, immune infiltration patterns, and potential responses to immunotherapy (sig linked). These findings support the view that mitochondrial dysregulation may be related to the intrinsic tumor behavior and the biological state of the tumor microenvironment [23]. Among the five genes in this model, COX7A1, MTHFD1L, MTG1, SCO2, and ACP6 all have reasonable biological associations with tumor progression (bio rel). COX7A1 is involved in mitochondrial respiratory chain function and may affect metabolic flexibility and treatment response [24, 25]. We analyzed that the increased expression of COX7A1 is related to poor prognosis, which may contribute to the performance of aggressive bladder cancer. MTHFD1L is a key enzyme in mitochondrial one-carbon metabolism, related to nucleotide synthesis, redox balance, and tumor progression [26-30]. Its single-cell T cell enrichment may also play a role in shaping the immune background of the tumor microenvironment. MTG1 is necessary for mitochondrial ribosome assembly and normal oxidative phosphorylation [31, 32]. Previous studies have shown that MTG1 may be related to poor prognosis of bladder cancer [33, 34], and our results are consistent with this. SCO2 is involved in the assembly of cytochrome c oxidase, as well as in mitochondrial energy metabolism and immune regulation related to macrophages [35, 36]. In this study, SCO2 is highly expressed in endothelial cells, and its role may go beyond that of tumor cells. ACP6 is involved in phospholipid metabolism and inflammation regulation, and is related to immune cell infiltration in other tumor types [37]. These genes construct a biologically reasonable signature that links mitochondrial function to cancer progression. The main finding of this study is that the risk score is closely related to the stromal features. High-risk tumor stromal score is relatively high, and it is also positively correlated with fibroblast-related, stroma-body-related, extracellular matrix-related or collagen-related signals. Gene ontology (GO) and Kyoto Encyclopedia of Genes and Genomes (KEGG) analyses also support the enrichment of pathways related to extracellular matrix organization, cell-matrix adhesion and focal adhesion in the high-risk group. The results show that mitochondrial dysfunction may be associated with extracellular matrix remodeling, fibroblast activation and features related to the stroma-rich microenvironment. This microenvironment is often related to tumor progression, immune escape and reduced treatment sensitivity [38-40]. It is also found that the risk score is associated with different immune infiltration patterns. In the high-risk group, the number of activated CD4 memory T cells and some macrophage subsets is relatively large; the levels of CD8 T cells, activated dendritic cells, follicular helper T cells and monocytes are higher in the low-risk group. This pattern suggests that there may be an active but functionally suppressed immune microenvironment in the high-risk group, and the low-risk group may maintain characteristics more similar to effective anti-tumor immunity. In our view, this may help explain why some tumors with immune activity still show less favorable predicted responses to immunotherapy.

The analyses of IPS, TIDE, and IMVigor210 data further support the clinical relevance of the model. Patients in the low-risk group generally showed more favorable predicted responses to immunotherapy, and the prognostic effect of the model was also confirmed in the IMVigor210 cohort. Although TMB did not differ significantly between the two risk groups, the risk score remained prognostically informative across TMB strata. These observations suggest that the five-gene signature may provide information that is complementary to conventional immunotherapy-related biomarkers.

Single-cell RNA sequencing analysis provided additional biological context. The cell type-specific expression patterns of COX7A1, MTHFD1L, and SCO2 suggest that mitochondria-related

genes may contribute to BLCA progression through different cellular compartments of the tumor microenvironment. In particular, the enrichment of Add1 in fibroblasts and the stromal associations identified in bulk transcriptomic analyses are consistent with the view that fibroblast-rich niches may be involved in the biology captured by the risk model.

Compared with single-gene biomarkers, multigene signatures may better reflect the complexity of tumor biology. In this study, the five-gene mitochondria-associated model provided prognostic information and was linked to both stromal and immune features, indicating potential value for risk stratification in bladder cancer. At the same time, our results should be interpreted cautiously because the present study was based mainly on public datasets and bioinformatic analyses.

Limitations

This study has several limitations. First, all analyses were based on retrospective public datasets, so the robustness of the model needs to be confirmed in prospective cohorts. The conclusion mainly comes from computational analysis; thus, experimental verification is still needed. Although the five-gene marker is associated with prognosis and tumor microenvironment characteristics, the potential biological mechanism still needs to be clarified. Further research is needed to verify these findings and explore the functional roles of these genes in bladder cancer.

Conclusions

Construction of a five-gene BTCC prognosis signature found COX7A1, MTHFD1L, MTG1, SCO2, and ACP6. The resulting risk score was associated with overall survival, stromal activation, immune-related characteristics, and predicted immunotherapy response. These findings suggest that the gene signature may be useful for prognostic stratification and for characterizing microenvironmental heterogeneity in BLCA.

Disclosure of conflict of interest

None.

Address correspondence to: Lingang Zhang, Emergency Department, Yuncheng Central Hospital, No. 3690 Hedong East Street, Yanhu District, Yuncheng 044000, Shanxi, China. E-mail: 125762265@qq.com

References

[1] Jiang X, Xia Y, Meng H, Liu Y, Cui J, Huang H, Yin G and Shi B. Identification of a nuclear mitochondrial-related multi-genes signature to predict the prognosis of bladder cancer. Front Oncol 2021; 11: 746029.

[2] Peng S, Ma S, Yang F, Xu C, Li H, Lu S, Zhang J, Jiao J, Han D, Shi C, Zhang R, Yang AG, Zhang K, Wen W and Qin W. Prognostic value and underlying mechanism of autophagy-related genes in bladder cancer. Sci Rep 2022; 12: 2219.

[3] Yan Z, Liu Y, Wang M, Wang L, Chen Z and Liu X. A novel signature constructed by mitochondrial function and cell death-related gene for the prediction of prognosis in bladder cancer. Sci Rep 2024; 14: 14667.

[4] Peng Y, Liu C, Li M, Li W, Zhang M, Jiang X, Chang Y, Liu L, Wang F and Zhao Q. Identification of a prognostic and therapeutic immune signature associated with hepatocellular carcinoma. Cancer Cell Int 2021; 21: 98.

[5] Wang P, Li J, Wu M, Ye M, Huang K and Zhu X. Human mitochondrial ribosomal RNA modification-based classification contributes to discriminate the prognosis and immunotherapy response of glioma patients. Front Immunol 2021; 12: 722479.

[6] Minnar CM, Chariou PL, Horn LA, Hicks KC, Palena C, Schlom J and Gameiro SR. Tumor-targeted interleukin-12 synergizes with entinostat to overcome PD-1/PD-L1 blockade-resistant tumors harboring MHC-I and APM deficiencies. J Immunother Cancer 2022; 10: e004561.

[7] Chang J, Wu H, Wu J, Liu M, Zhang W, Hu Y, Zhang X, Xu J, Li L, Yu P and Zhu J. Constructing a novel mitochondrial-related gene signature for evaluating the tumor immune microenvironment and predicting survival in stomach adenocarcinoma. J Transl Med 2023; 21: 191.

[8] Rath S, Sharma R, Gupta R, Ast T, Chan C, Durham TJ, Goodman RP, Grabarek Z, Haas ME, Hung WHW, Joshi PR, Jourdain AA, Kim SH, Kotrys AV, Lam SS, McCoy JG, Meisel JD, Miranda M, Panda A, Patgiri A, Rogers R, Sadre S, Shah H, Skinner OS, To TL, Walker MA, Wang H, Ward PS, Wengrod J, Yuan CC, Calvo SE and Mootha VK. MitoCarta3.0: an updated mitochondrial proteome now with sub-organelle localization and pathway annotations. Nucleic Acids Res 2021; 49: D1541-D1547.

[9] Wu T, Hu E, Xu S, Chen M, Guo P, Dai Z, Feng T, Zhou L, Tang W, Zhan L, Fu X, Liu S, Bo X and

Yu G. clusterProfiler 4.0: a universal enrichment tool for interpreting omics data. Innovation (Camb) 2021; 2: 100141.
[10] Wang T, Zhou Z, Wang X, You L, Li W, Zheng C, Zhang J, Wang L, Kong X, Gao Y and Sun X. Comprehensive analysis of nine m7G-related lncRNAs as prognosis factors in tumor immune microenvironment of hepatocellular carcinoma and experimental validation. Front Genet 2022; 13: 929035.
[11] Mootha VK, Lindgren CM, Eriksson KF, Subramanian A, Sihag S, Lehar J, Puigserver P, Carlsson E, Ridderstråle M, Laurila E, Houstis N, Daly MJ, Patterson N, Mesirov JP, Golub TR, Tamayo P, Spiegelman B, Lander ES, Hirschhorn JN, Altshuler D and Groop LC. PGC-1alpha-responsive genes involved in oxidative phosphorylation are coordinately downregulated in human diabetes. Nat Genet 2003; 34: 267-273.
[12] Subramanian A, Tamayo P, Mootha VK, Mukherjee S, Ebert BL, Gillette MA, Paulovich A, Pomeroy SL, Golub TR, Lander ES and Mesirov JP. Gene set enrichment analysis: a knowledge-based approach for interpreting genome-wide expression profiles. Proc Natl Acad Sci U S A 2005; 102: 15545-15550.
[13] Zhao HB, Zeng YR, Han ZD, Zhuo YJ, Liang YK, Hon CT, Wan S, Wu S, Dahl D, Zhong WD and Wu CL. Novel immune-related signature for risk stratification and prognosis in prostatic adenocarcinoma. Cancer Sci 2021; 112: 4365-4376.
[14] Krøigård AB, Thomassen M, Lænkholm AV, Kruse TA and Larsen MJ. Evaluation of nine somatic variant callers for detection of somatic mutations in exome and targeted deep sequencing data. PLoS One 2016; 11: e0151664.
[15] Fu J, Li K, Zhang W, Wan C, Zhang J, Jiang P and Liu XS. Large-scale public data reuse to model immunotherapy response and resistance. Genome Med 2020; 12: 21.
[16] Cerami E, Gao J, Dogrusoz U, Gross BE, Sumer SO, Aksoy BA, Jacobsen A, Byrne CJ, Heuer ML, Larsson E, Antipin Y, Reva B, Goldberg AP, Sander C and Schultz N. The cBio cancer genomics portal: an open platform for exploring multidimensional cancer genomics data. Cancer Discov 2012; 2: 401-404.
[17] Gao J, Aksoy BA, Dogrusoz U, Dresdner G, Gross B, Sumer SO, Sun Y, Jacobsen A, Sinha R, Larsson E, Cerami E, Sander C and Schultz N. Integrative analysis of complex cancer genomics and clinical profiles using the cBioPortal. Sci Signal 2013; 6: pl1.
[18] Hao Y, Hao S, Andersen-Nissen E, Mauck WM 3rd, Zheng S, Butler A, Lee MJ, Wilk AJ, Darby C, Zager M, Hoffman P, Stoeckius M, Papalexi E, Mimitou EP, Jain J, Srivastava A, Stuart T, Fleming LM, Yeung B, Rogers AJ, McElrath JM, Blish CA, Gottardo R, Smibert P and Satija R. Integrated analysis of multimodal single-cell data. Cell 2021; 184: 3573-3587, e3529.
[19] Lai H, Cheng X, Liu Q, Luo W, Liu M, Zhang M, Miao J, Ji Z, Lin GN, Song W, Zhang L, Bo J, Yang G, Wang J and Gao WQ. Single-cell RNA sequencing reveals the epithelial cell heterogeneity and invasive subpopulation in human bladder cancer. Int J Cancer 2021; 149: 2099-2115.
[20] Hafemeister C and Satija R. Normalization and variance stabilization of single-cell RNA-seq data using regularized negative binomial regression. Genome Biol 2019; 20: 296.
[21] Cazier JB, Rao SR, McLean CM, Walker AK, Wright BJ, Jaeger EE, Kartsonaki C, Marsden L, Yau C, Camps C, Kaisaki P; Oxford-Illumina WGS500 Consortium, Taylor J, Catto JW, Tomlinson IP, Kiltie AE and Hamdy FC. Whole-genome sequencing of bladder cancers reveals somatic CDKN1A mutations and clinicopathological associations with mutation burden. Nat Commun 2014; 5: 3756.
[22] Yu SH, Kim SS, Lee H, Kim S and Kang TW. Somatic mutation of the non-muscle-invasive bladder cancer associated with early recurrence. Diagnostics (Basel) 2023; 13: 3201.
[23] Xiong H, Lin C, Huang X and Wang H. A novel mitochondrial-related lncRNA signature mediated prediction of overall survival, immune landscape, and the chemotherapeutic outcomes for bladder cancer patients. Discov Oncol 2024; 15: 239.
[24] Feng Y, Xu J, Shi M, Liu R, Zhao L, Chen X, Li M, Zhao Y, Chen J, Du W and Liu P. COX7A1 enhances the sensitivity of human NSCLC cells to cystine deprivation-induced ferroptosis via regulating mitochondrial metabolism. Cell Death Dis 2022; 13: 988.
[25] Wang SY, Yang XQ, Wang YX, Shen A, Liang CC, Huang RJ, Cheng UH, Jian R, An N, Xiao YL, Wang LS, Zhao Y, Lin C, Wang CP, Yuan ZP and Yuan SQ. Overexpression of COX7A1 promotes the resistance of gastric cancer to oxaliplatin and weakens the efficacy of immunotherapy. Lab Invest 2024; 104: 102090.
[26] Eich ML, Rodriguez Pena MDC, Chandrashekar DS, Chaux A, Agarwal S, Gordetsky JB, Ferguson JE, Sonpavde GP, Netto GJ and Varambally S. Expression and role of methylenetetrahydrofolate dehydrogenase 1 like (MTHFD1L) in bladder cancer. Transl Oncol 2019; 12: 1416-1424.
[27] Sial N, Rehman JU, Saeed S, Ahmad M, Hameed Y, Atif M, Rehman A, Asif R, Ahmed H, Hussain MS, Khan MR, Ambreen A and Ambreen A. Integrative analysis reveals methylenetetrahydrofolate dehydrogenase 1-like as

an independent shared diagnostic and prognostic biomarker in five different human cancers. Biosci Rep 2022; 42: BSR20211783.
[28] Ieranò C, Righelli D, D'Alterio C, Napolitano M, Portella L, Rea G, Auletta F, Santagata S, Trotta AM, Guardascione G, Liotti F, Prevete N, Maiolino P, Luciano A, Barbieri A, Di Mauro A, Roma C, Esposito Abate R, Tatangelo F, Pacelli R, Normanno N, Melillo RM and Scala S. In PD-1+ human colon cancer cells NIVOLUMAB promotes survival and could protect tumor cells from conventional therapies. J Immunother Cancer 2022; 10: e004032.
[29] Liu X, Mei W, Padmanaban V, Alwaseem H, Molina H, Passarelli MC, Tavora B and Tavazoie SF. A pro-metastatic tRNA fragment drives Nucleolin oligomerization and stabilization of its bound metabolic mRNAs. Mol Cell 2022; 82: 2604-2617, e2608.
[30] Fujihara KM, Zhang BZ, Jackson TD, Ogunkola MO, Nijagal B, Milne JV, Sallman DA, Ang CS, Nikolic I, Kearney CJ, Hogg SJ, Cabalag CS, Sutton VR, Watt S, Fujihara AT, Trapani JA, Simpson KJ, Stojanovski D, Leimkühler S, Haupt S, Phillips WA and Clemons NJ. Eprenetapopt triggers ferroptosis, inhibits NFS1 cysteine desulfurase, and synergizes with serine and glycine dietary restriction. Sci Adv 2022; 8: eabm9427.
[31] Kim HJ and Barrientos A. MTG1 couples mitoribosome large subunit assembly with intersubunit bridge formation. Nucleic Acids Res 2018; 46: 8435-8453.
[32] Kim HJ and Barrientos A. Mitochondrial MTG1 is necessary for proper human cardiomyocyte activity and zebrafish cardiac development. Comment to "Novel role of mitochondrial GTPases 1 in pathological cardiac hypertrophy". J Mol Cell Cardiol 2019; 129: 1.
[33] Wu Y, Liu Z, Wei X, Feng H, Hu B, Liu B, Luan Y, Ruan Y, Liu X, Liu Z, Wang S, Liu J and Wang T. Identification of the functions and prognostic values of RNA binding proteins in bladder cancer. Front Genet 2021; 12: 574196.
[34] Maiti P, Antonicka H, Gingras AC, Shoubridge EA and Barrientos A. Human GTPBP5 (MTG2) fuels mitoribosome large subunit maturation by facilitating 16S rRNA methylation. Nucleic Acids Res 2020; 48: 7924-7943.
[35] Ruan X, Cao M, Yan W, Jones YZ, Gustafsson ÅB, Patel HH, Schenk S and Wang SE. Cancer-cell-secreted extracellular vesicles target p53 to impair mitochondrial function in muscle. EMBO Rep 2023; 24: e56464.
[36] Li L, Han L and Qu Z. NF-κB RelA is a cell-intrinsic metabolic checkpoint restricting glycolysis. Cell Biosci 2024; 14: 11.
[37] Qiu R, Lei Y, Yang Q, Zeng J, Zhou Y, Sun B and Sun Y. Identification and functional analysis of lysophosphatidic acid phosphatase type 6 (ACP6) gene in golden pompano (Trachinotusovatus). Fish Shellfish Immunol 2024; 154: 109904.
[38] Izzi V, Davis MN and Naba A. Pan-cancer analysis of the genomic alterations and mutations of the matrisome. Cancers (Basel) 2020; 12: 2046.
[39] Labani-Motlagh A, Ashja-Mahdavi M and Loskog A. The tumor microenvironment: a milieu hindering and obstructing antitumor immune responses. Front Immunol 2020; 11: 940.
[40] Gok Yavuz B, Gunaydin G, Kosemehmetoglu K, Karakoc D, Ozgur F and Guc D. The effects of cancer-associated fibroblasts obtained from atypical ductal hyperplasia on anti-tumor immune responses. Breast J 2018; 24: 1099-1101.